IEEE Access
Multidisciplinary | Rapid Review | Open Access Journal

Received July 26, 2019, accepted August 11, 2019, date of publication August 16, 2019, date of current version August 29, 2019.

Digital Object Identifier 10.1109/ACCESS.2019.2935761

Landslide Detection Using Residual Networks and the Fusion of Spectral and Topographic Information

MAHER IBRAHIM SAMEEN[1] AND BISWAJEET PRADHAN[1,2], (Senior Member, IEEE)

[1]Centre for Advanced Modelling and Geospatial Information Systems (CAMGIS), Faculty of Engineering and Information Technology, University of Technology Sydney, Ultimo, NSW 2007, Australia

[2]Department of Energy and Mineral Resources Engineering, Sejong University, Seoul 05006, South Korea

Corresponding author: Biswajeet Pradhan (biswajeet.pradhan@uts.edu.au)

This work was funded by the Centre for Advanced Modelling and Geospatial Information Systems (CAMGIS), University of Technology Sydney, under Grant 323930, Grant 321740.2232335, Grant 321740.2232357, Grant 321740.2232424, and Grant 321740.2232452.

ABSTRACT Landslide inventories are in high demand for risk assessment of this natural hazard, particularly in tropical mountainous regions. This research designed residual networks for landslide detection using spectral (RGB bands) and topographic information (altitude, slope, aspect, curvature). Recent studies indicate that deep learning methods such as convolutional neural networks (CNN) improve landslide mapping results compared to traditional machine learning. But the effects of network architecture designs and data fusion remain largely underexplored in landslide detection. We compared a one-layer CNN with two of its deeper counterparts and residual networks with two fusion strategies (layer stacking and feature-level fusion) to detect landslides in Cameron Highlands, Malaysia. Sixteen different maps were created using proposed methods and evaluated in separate training and testing sub-areas based on overall accuracy, F1-score, and mean intersection over union (mIOU) metrics. When layer stacking is used as a fusion approach, none of the network designs improved landslide detection results. However, our findings showed that when using feature-level fusion, results could be enhanced with the same network designs. Residual networks performed best improving F1-score and mIOU by 0.13 and 12.96%, respectively, using feature-level fusion rather than layer stacking. CNN models also enhanced the detection outcome with the same fusion approach. On single modality datasets, models' performance varies according to input data, highlighting the effects of input data on network architecture selection. In general, residual networks found to converge faster and generalize better to test areas than other models tested in this research.

INDEX TERMS Landslide detection, deep learning, convolutional neural network, GIS, residual networks, remote sensing.

I. INTRODUCTION

Detection of landslides is an important task in hazard and risk studies and has attracted researchers' attention in recent years [1]–[9]. Landslide inventories require regular updates after major rainfall and seismic events. Information on past landslides is important to understand the causal factors involved and to predict future hazards [10], [11]. Remote sensing has been an economical solution for detecting landslides and updating existing landslide inventory databases. It provides a wide range of terrestrial data of different spatial and temporal resolution degrees. However, detecting landslides in remote sensing data is still a challenge and requires improvements [4].

Several studies have focused on field surveys and remote sensing image interpretation [12]–[14]. Prior knowledge plays an important role in determining the accuracy of inventory maps of landslides in these methods. They are also time-consuming and labour-intensive, especially in large areas [15]. Scientists, therefore, developed automated and semi-automated methods for remote sensing data to detect landslides. Some methods require bi-temporal aerial

The associate editor coordinating the review of this article and approving it for publication was Weimin Huang.

photographs [3], [16], [17], satellite images [18], [19] or point clouds [20] while others rely on post-event datasets [21]. Methods that combine data from different modalities also exist [22], [23]. Previous studies used very high-resolution images (spaceborne, airborne, and terrestrial) [24], point cloud or Light Detection and Ranging (LiDAR) [25]–[28], Synthetic Aperture Radar (SAR) [29] and Interferometric SAR (InSAR) [30], [31] for landslide inventory mapping (LIM).

II. PREVIOUS WORK

This research classifies LIM methods into three groups: pixel-based, object-based, and deep learning.

A. PIXEL-BASED METHODS

In pixel-based LIM methods, single pixels are the fundamental processing elements. Image correlation is a common method of landslide detection in remote sensing data based on single-pixel information [32]–[35]. Various factors affect the accuracy of these methods including imperfect sensor models, co-registration and orthorectification errors, and diversity in study site characteristics (vegetation cover, cast shadows) [36]. Reference [35] proposed a multiple pairwise image correlation technique to detect surface displacements more accurately. However, parallel processing and further improvements are required to address the computational efficiency and coarser spatial resolution in the current implementation. Reference [37] developed an intensity threshold and unsupervised classification of EO-1 and SPOT5 images for landslide detection. In [38], image saliency was used to detect landslides in Landsat images. Change detection is also widely used for the detection of landslides. It is straightforward and applies to large and small areas. Reference [39] presented a detailed review of several change detection techniques for remote sensing applications. Reference [3] applied the Markov random field for landslide detection from aerial photographs. Reference [23] combined optical and polarimetric SAR data in vegetated areas with LIM change detection methods. Reference [19] detected landslides on the basis of pre-and post-disaster COSMO-SkyMed images. More recently, [29] performed LIM using airborne X-band SAR data before and after the event. Machine learning has also recently been applied to LIM using pixel-based approaches. Mezaal and Pradhan 2018 proposed a data mining-aided method for automatic landslide detection in rainforest areas. Reference [21] used AIRSAR data to apply support vector machine and index of entropy models for LIM. The random forest has been used in [40] based on texture characteristics taken from Landsat 8 images.

Overall, pixel-based methods often require extensive parametric tuning and precise geometrical correction or co-registration while simple and applicable to large areas. Noise and outliers also have major effects on the accuracy of these methods, in particular, if training data is required to learn model parameters (e.g. machine learning).

B. OBJECT-BASED METHODS

Object-based LIM depends not only on single pixels but also on image objects. An image object is a pixel collection with similar spectral signatures [41], [42]. Object-based image analysis or OBIA allows extracting statistical, textural, contextual, and geometrical features that can help distinguish objects not possible by single pixels [16]. OBIA has successfully been applied to many applications of remote sensing, such as image classification [43]–[45], image segmentation [46] and object detection [44]. OBIA was mainly used in the field of landslide studies to delineate landside boundaries and to take advantages of multi-resolution images and features in different modalities. Reference [47] investigated the spectral, spatial, and morphometric properties of landslides with OBIA and (Resourcesat-1, DEM) data. The accuracy of OBIA methods is greatly influenced by segmentation parameters. In a separate paper, [48] optimized OBIA segmentation process for landslide detection with plateau objective function derived from the analysis of spatial autocorrelation and intra-segment variance. Many researchers have tried OBIA in combination with other methods such as random forest [4], [43], [49], change detection [50], and genetic algorithms [51]. Landslide detection also performed by combining digital elevation models (DEM) and optical ortho-images [34]. Reference [52] used multi-resolution optical images to address the problem of high-resolution images with the landslide heterogeneity in LIM. Reference [53] compared OBIA based LIM methods using polarimetric SAR and optical satellite imagery. Debris flows and riverbeds were best detected with the SAR data, while only optical images could detect individual landslides. In [4], LiDAR and QuickBird data are combined by OBIA for landslide detection. More recently, [9] used optimized OBIA and machine learning to detect landslides in rainforest areas using LiDAR and orthophotos. In another study, [54] used Dempster-Shafer to improve OBIA outputs from different machine learning models.

While OBIA offers extra features that distinguish landslides from other objects, however, it needs to optimize segmentation parameters (e.g. scale) [55] and in these methods, the degree of automation is low compared to pixel-based methods.

C. DEEP LEARNING METHODS

Researchers are constantly trying to untangle the combination of remote sensing images and topographical factors (e.g., altitude, slope, curvature) that best discriminate landslides from other objects. To the extent that landslides do not have unique spectral signatures and unique shapes, it may be useful to combine features from different modalities to detect landslides in complex areas (e.g., rainforest). Both pixel and object-based methods have limitations in addressing this problem. Several methods based on deep learning have recently been proposed for the detection of landslides. Reference [56] used convolutional neural networks (CNN) with average and maximum pooling for automatic landslide

detection based on texture change detection. Reference [6] used a deep CNN in combination with change detection methods for landslide mapping. Landslides occur over a wide variety of spatial and temporal scales [17]. Typical CNN models with global pooling that have disadvantages in extracting features on multiple scales, therefore, need improvements in design. To address the complexity and spatial uncertainty of landslides, [17] developed a CNN model with pyramid pooling instead of global pooling for LIM. Their model could explore the context of images efficiently and better detect landslides on various scales. Reference [8] compared various traditional machine learning for landslide detection with deep learning methods. Their results suggest that if CNN well designed and its hyperparameters are carefully optimized, it may perform better than other machine learning methods. Its accuracy depends heavily on layer depth, input window sizes and training strategies. Reference [28] proposed recurrent neural networks to use LiDAR, orthophoto, and textural features to detect landslides and found them to be effective in combining these features.

Studies using deep learning to detect landslides are limited, and it is hard to make any conclusive statements about their performance compared to other pixel and object-based models. However, given their powerful ability to extract features from images, they may be a good choice for detecting landslides in data from different modes.

This research proposes a CNN model with residual blocks to effectively detect landslides from combined aerial photography and LiDAR data. The main contribution of this study is designing a residual network with few convolutional layers that can extract complementary features from aerial photographs and topographic factors.

III. METHODOLOGY

This section discusses the study area, datasets and the techniques proposed, and the techniques used as comparative standards.

A. DESCRIPTION OF THE STUDY AREA

The study area of this research is Cameron Highlands in Malaysia Peninsula owing to frequent occurrence of landslides (Figure 1). It is about 200 km from the capital city of Kuala Lumpur at the north-eastern tip of Pahang State. It is a tropical mountainous area with frequent mass movement and flash floods caused by heavy and prolonged precipitation [10], [57]. The combination of the topography, climate and illegal human activities create natural hazards which pose a major threat in Cameron Highlands. Government reports and previous research indicate that landslides in this area have been common and there have been significant damages to properties in the past. The area's geomorphology is hilly (mainly the western and north-western parts), and altitudes range from 840 m to 2110 m. The main vegetation cover of the area is forest and tea plantations, temperate vegetable and flower farms. The primary lithology in this area is the

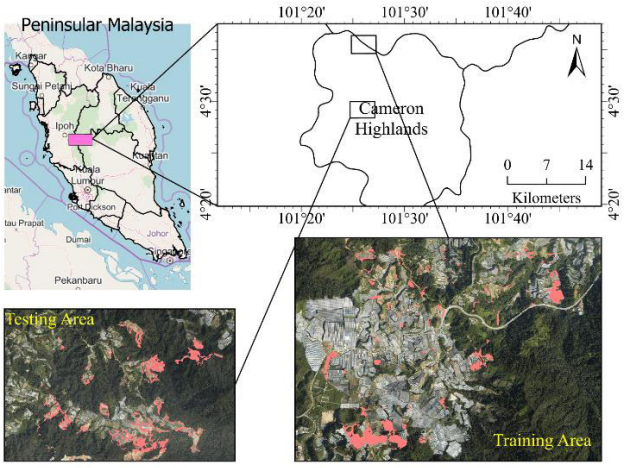

FIGURE 1. The geographic location of the study area and selected training and testing sites.

megacrystic biotite granites, the other geological structures being schists, phyllite, [10].

Cameron Highlands is located in the moderate climate with average annual rainfall between March and May and from November to December. Average daytime and night-time temperatures in the study area are 24 °C and 14 °C, respectively. In terms of land use, approximately 8% (5,500 ha) of the study area is agricultural land, 86% (60,000 ha) is cultivated, 4% (2,750 ha) are housed, and the remainder is used for recreation and other activities.

B. SELECTED TRAINING AND TESTING SITES

LiDAR point clouds with an 8 points/m2 density and a 25,000 Hz pulse frequency rate were acquired over the study areas by an airborne system on 15 January 2015. The absolute vertical and horizontal precisions were 0.15 m and 0.3 m, respectively. Orthophotos were acquired using the same system and time. A digital elevation model (DEM) with 1 m spatial resolution was created from the LiDAR data. The aerial orthophotos had 10 cm ground accuracy but were resampled to 1 m. The DEM was created after removing the non-ground points by the multi-scale curvature algorithm and IDW (Inverse Distance Weighted) interpolation techniques implemented in ArcGIS Pro 2.4. Subsequently, geomorphological parameters such as slope, aspect, total curvature were derived at the same spatial resolution. On the other hand, a landslide inventory was prepared based on an existing inventory map prepared by [10], [28].

Two subset areas were chosen in Cameron Highlands based on the available data, landslide inventory and shape/size variations. Figure 1 shows these areas within Cameron Highlands. The first area covers 10.50 km^2 and is considered the training area. It contains about 152 landslide inventories represented by polygons. The altitude ranges from 1068 m to 1736 m. Most of this area is hilly and the slope between flatlands to 70 degrees. The second area covers about 9.83 km^2 and is considered the testing area in this research. It contains 121 landslides represented by polygons.

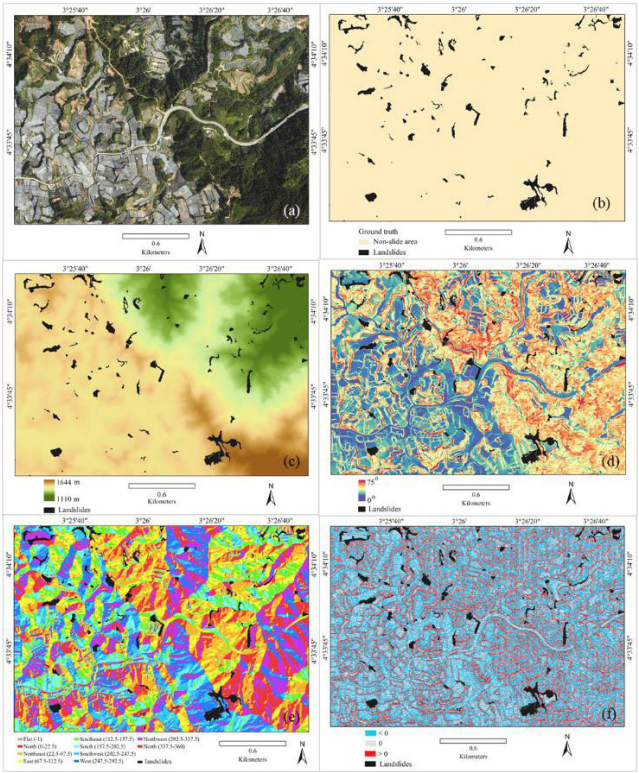

FIGURE 2. (a) Aerial photograph, (b) ground truth, (c) altitude, (d) slope, (e) aspect, and (f) total curvature for the test sub-area.

The area's altitude ranges from 1110 m and 1644 m. Slope values range from flat to 75 degrees. Figure 2 shows the aerial photograph, ground truth map, and maps of the topographical variables for the test area. Our discussions and final assessment are on this test area as we aim to avoid overfitting or underfitting effects.

C. SELECTED TRAINING AND TESTING SITES

Our database contained an aerial photo (1 m resolution) and four topographical variables (altitude, slope, aspect, and curvature) all with the same resolution for both training and testing areas. All the raster had the same dimensions (2926×3588 for the training area and 2526×3892 for the testing area). CNN models require the dimensions to be divisible by the patch size (15×15 pixels). The patch size was selected by a trial and error method. The rasters, therefore, were zero-padded to be divisible by the patch size used in this research. The pixel values in the raster datasets were normalized using the minimum and maximum values in the dataset. The test datasets were normalized based on the minimum and maximum values obtained from the training area. The labels (0 for non-slides, 1 for landslides) were encoded using one-hot encoding to become [1, 0] for non-slides and [0, 1] for landslides.

D. PROPOSED MODELS

1) CONVOLUTIONAL NEURAL NETWORKS (CNN)

CNNs are a powerful family of neural networks for image recognition in particular. They were first introduced by [58] and improved substantially after computing resources and software have become accessible. CNNs benefit from the properties of the natural signals of local connections shared weights, combination and use of a wide range of layers [59]. Consequently, they are efficient feature extractors of images without the need to craft complex rules.

Convolutional layers are the main component of these models which are composed of a set of convolutional kernels associated with a small area of the input image known as a patch. For a given image ($I_{x,y}$), the convolution operation is performed according to $F_l^k = \left(I_{x,y}.K_l^k\right)$ where x, y shows the spatial locality, K_l^k represents l^{th} convolutional kernel of the k^{th} layer. Pooling layers used to summarize information across adjacent spatial regions. Two common functions used in the pooling operation are average and maximum pooling. For each patch in the feature map, the former calculates the average value while the latter sums each patch of the feature map to the maximum value. There are also global pooling layers that sample the entire feature map to a single value. Pooling improves model invariance to local translation and reduces model parameters. They are calculated using $Z_l = f_p\left(F_{x,y}^l\right)$ where Z_l represents l^{th} output feature map, $F_{x,y}^l$ is the l^{th} input feature map and $f_p(.)$ defines the type of pooling operation. Activation functions add non-linearity to the model as are defined as $T_l^k = f_A\left(F_l^k\right)$ where F_l^k is an output of a convolution operation, $f_A(.)$ defines the activation function and T_l^k being the transformed output for k^{th} layer. ReLU is the most common activation function as it helps to overcome the vanishing gradient problem. Batch normalization and dropout are techniques used as layers in modern network architecture to speed up the convergence and introduce regularization within the network [60]. Both improve the generalization of the network. Dense layers or fully connected layers are mostly applied at the end of the network for classification purposes and they are global operations. Next, we explain our proposed network architectures for the detection of landslides.

2) BASELINE CNN MODELS

Figure 3 shows the architectures of our proposed baseline models. The first model is a one-layer CNN composed of seven total layers including the input and output (Figure 3a). The input data are first fed into a 3×3 convolution with no padding and a stride of 1 as the kernel moves across the input data. We use ReLU (rectified linear unit) as an activation function because it is successful in CNN models. The output feature maps are made more abstract by a maximum pooling layer with a pool size of 2×2. The produced feature maps are subsequently flattened to a suitable dimension. A dense layer is used before the softmax classification layer with ReLU activation. Between the last two layers, a dropout layer with 0.3 elimination fraction was used to apply regularization and avoid overfitting to training data. The model output is one-hot encoded predictions which are then transformed respectively to 0 (non-slide) and 1 (landslide). The second and third

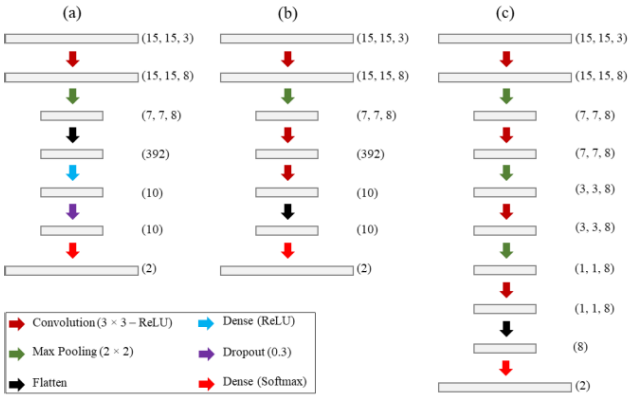

FIGURE 3. The network architecture of the CNN baselines used in this research.

models are motivated by the architectures developed by [8] for landslide detection in Nepal (Figure 3a, 3b). The second CNN has also seven total layers but with 3 convolutions and without dense and dropout layers. The third model has 10 total layers with four convolutions and 3 max pooling.

3) PROPOSED RESIDUAL NETWORK

Residual networks (or ResNet) are first introduced by [61] as an optimal methodology to train deep networks. The model won the 2015-ILSVRC competition. They are computationally more efficient than previously proposed networks. Adding more layers to a CNN model does not ensure better prediction ability and makes the network less expressive. ResNet improves on these issues by a residual block or identity shortcut connection defined as $H(x) = F(x, \{W_i\}) + W_s x$ where x and H(x) are the input and output of the residual block, F(.) represents the residual mapping function to be learned, W_i and W_s are the convolutional layers parameters and linear project matrix, respectively. Figure 4 depicts our proposed ResNet for the detection of landslides. It is composed of 9 total layers with one residual block of 7 total layers. The network starts by getting an input ($I_{x,y}$) and applies a 3 × 3 convolution and max-pooling of 2 × 2 and produces an output. This then goes into a batch normalization layer and a ReLU activation. The output from these sequential operations become the input (x) to the residual block. The residual block applies a series of operations like batch normalization, ReLU, 3 × 3 convolution, batch normalization, ReLU, 3 × 3 convolution on the received input. The output of these sequential operations added together with the input to produce an output (H(x)). Then batch normalization, ReLU, global average pooling, dropout with 0.3 elimination fraction, and dense (softmax) operations were performed to produce the detection result.

4) FUSION TECHNIQUES

Two fusion methods were used to detect landslides from spectral data and four topographical variables (Figure 5). The first fusion method uses layer stacking to fuse the spectral bands with four topographical variables to produce a

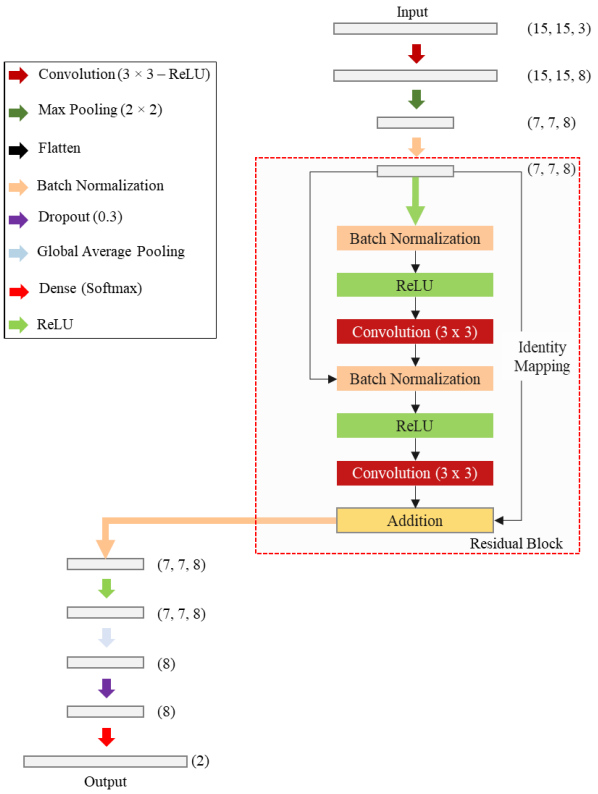

FIGURE 4. The proposed architecture of the residual network.

7-band composite raster. Before stacking, the datasets were normalized to account for differences between image values and topographical variables. After preprocessing the 7-band raster, four network models of different architectures were trained and tested. The second fusion method uses network models as feature extractors to transform the spectral data and topographical variables into abstract representations before classifying. The fusion was performed using the features learned by dense (ReLU) layers or the features produced after flattening operation. In our research, the decision tree model was used as a classification technique that takes the extracted features by the network models and produces the detection outcome.

5) TRAINING METHODOLOGY

Deep learning algorithms are mostly trained with stochastic gradient descent (SGD) by backpropagation because it uses easy mathematical tricks (e.g., differentiation or chain rules) to efficiently minimize a differentiable objective function with respect to the model's parameters. Recently several improvements have been proposed for the mini-batch SGD. We use adaptive moment estimation (Adam) which is an optimization approach that computes adaptive learning rates for each parameter of a network model. The technical details of Adam can be found in the original paper [62]. In this research, it was used to minimize the binary cross-entropy loss (Equation 1). All the weights are initialized using a zero-mean Gaussian distribution with a standard deviation

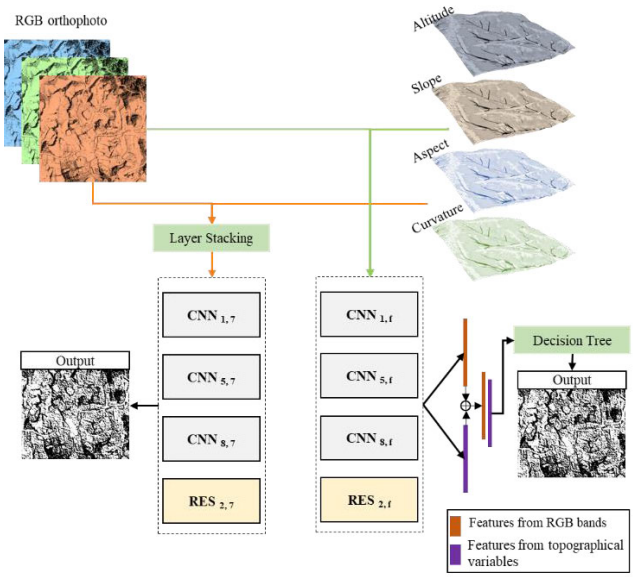

FIGURE 5. Fusion approaches used to combine spectral and topographical variables.

0.01, and the biases are initialized with constant 1. The training uses a batch size of 512. The learning rate is initially set to 0.001 and sigmoidal decay was used as a learning rate policy. The models are trained for 500 iterations with early termination. If no improvement noted in the validation accuracy for 10 iterations, the training process is automatically terminated.

$$\text{loss}\left(\hat{y}, y\right) = -\frac{1}{m}\sum_{i=1}^{m} y^{(i)} \log \hat{y}^{(i)} + \left(1 - y^{(i)} \log\left(1 - \hat{y}^{(i)}\right)\right) \tag{1}$$

IV. RESULTS

A. EXPERIMENTAL SETTING

Two study sites as described in Section 3.1 were used to evaluate the proposed models and conducting comparative assessments with other benchmark methods. However, the evaluations and the discussions of this paper is based on the model's performance obtained on the basis on the testing site.

Based on the accessible datasets outlined previously in this article, three experiments were designed to justify our proposed approach. First, various models were trained on (i) only spectral bands acquired from aerial photography, (ii) only topographical variables (e.g., altitude, slope, aspect, and curvature), and (iii) both spectral bands and the four topographical variables. Second, to assess the effectiveness of modelling on multimodal data fusion for landslide detection, we evaluated CNN and ResNet architectures. Third, models with different depths were tested to evaluate the complexity needed for the identification of landslides where spectral bands, topographical variables, or both are available. All the experiments have been developed using open source libraries such as scikit-learn, Keras, and gdal in Python. They all performed using a single GeForce MX130 GPU. Overall, sixteen landslide maps were generated using various CNN and ResNet models. In CNNp, q models, the index of p is the number of convolutional layers, and q is the number of raster bands. ResNet2, q models use only two convolutional layers, so p is 2. When the models use multimodal fusion, q is replaced with f, indicating the fusion of spectral bands and the topographical factors. The source code of the models is available upon reasonable request from the corresponding author.

Various evaluation metrics including overall accuracy, F1-score, and the mean Intersection Over Union (mIOU) were used to evaluate the predictive efficiency of the proposed and other benchmark models. Overall accuracy is only used to obtain general insight about the predictive performance of the models on the training and validation subsets during the training phase. F1-score $2 \times \text{precision} \times \text{recall}/(\text{precision} + \text{recall})$ uses precision and recall assessing the performance of a trained model. The former relies on True Positives (TPs) and False Positives (FPs), while the latter is based on False Negatives (FNs) and TPs. This implies that precision measures the prediction accuracy of the models and recall evaluate how precise the models are in finding all the pixels in the ground truth belong to landslides. We also used mIOU in addition to these metrics as it is a standard evaluation metric in semantic segmentation and landslide detection studies [8]. Equation 2 shows the formula for computing mIOU.

$$\text{mIOU} = \frac{1}{k+1}\sum_{i=0}^{k} \frac{p_{ii}}{\sum_{j=0}^{k} p_{ij} + \sum_{j=0}^{k} p_{ji} - p_{ii}} \tag{2}$$

where $k+1$ ($k=1$ in this research) is the number of classes, i is the label of the ground truth, and the j is the label of the prediction. The p_{ij} is the total number of pixels labelled as j but predicted as i.

B. LANDSLIDE DETECTION RESULTS

A total of sixteen landslide maps for comparison purposes were produced using the models suggested and others exist in the recent literature [8]. A range of four one-layer CNN models using spectral bands, four topographical variables (altitude, slope, aspect, curvature), a layer stacking of the datasets, and data fusion on a feature level was applied. Similarly, 5 and 8-layer CNN models have been trained on the same datasets for the accuracy assessment of network depth effects. Finally, 4 ResNet models were implemented on the same datasets with 2 convolutional layers. Figure 6 shows the produced landslide maps by the implemented models. These results are explained in more detail in the following paragraphs.

C. EVALUATION OF PROPOSED MODELS WITH DIFFERENT DATASETS

In this experiment, we assessed the predictive ability of the models proposed for the detection of landslides in spectral

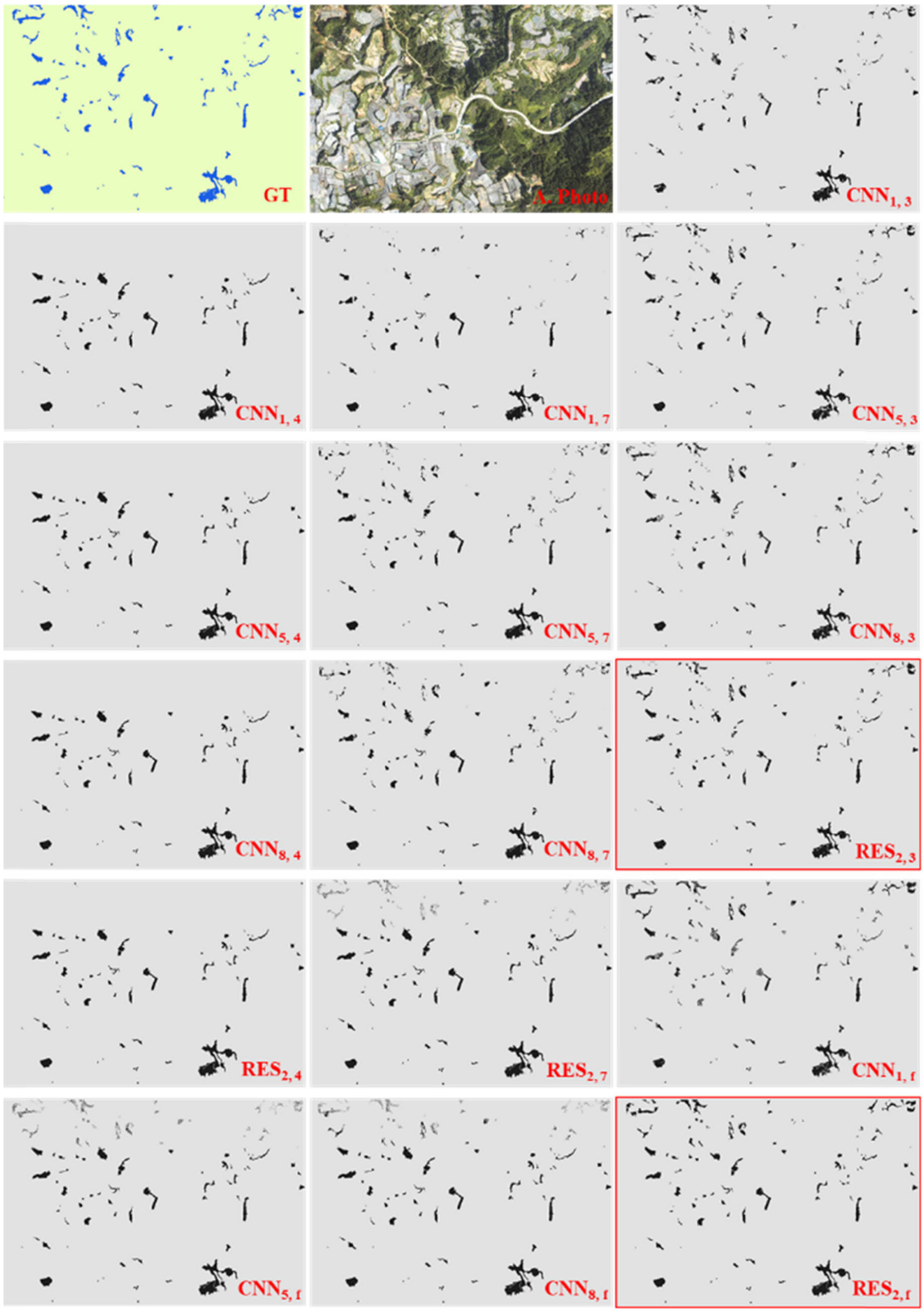

FIGURE 6. Results of LIM using various CNN and ResNet models with multimodal fusion and without.

bands, topographical variables and the combination of both datasets. Landslides could be identified based on spectral bands. Extra topographical variables could promote detection results only when using feature-level fusion (Figure 7). Spectral bands allowed more accurate detection of landslides than the use of topographical variables. However,

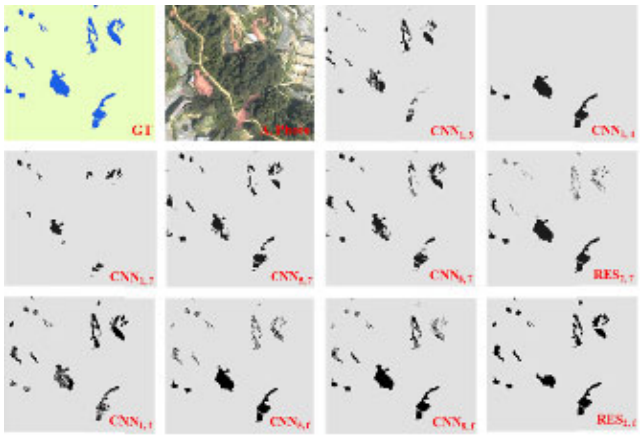

FIGURE 7. Enlarged maps of a subset area from the test area. In CNNp, q models, the index of p is the number of a convolutional layer, and q is the number of raster bands. RES2, q models use only two convolutional layers, so p is 2. When the models use multimodal fusion, q is replaced with f, indicating the fusion of spectral bands and the topographical factors.

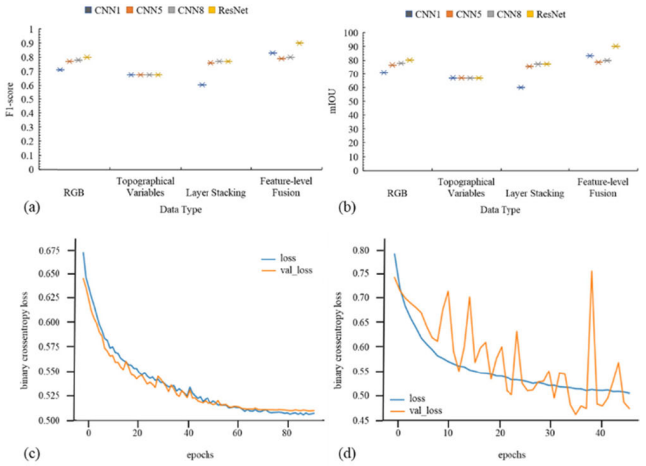

FIGURE 8. (a) Impacts of input data type on models F1-score, (b) impacts of input data type on models mIOU, (c) learning curve of the CNN1, 3, and (d) learning curve of the RES2, 3.

topographical variables could reduce the salt-and-pepper like noise in the detection results. For CNN1, 3, the mIOU is 70.86% and F1-score is 0.710 but CNN1, 4 only achieved 66.91% mIOU and 0.670 F1-score. Fusion by layer stacking of spectral bands and topographical variables could not enhance the results of the detection. For example, the CNN1, 7 did less than using single datasets (mIOU = 60.01%, F1-score = 0.600). Even deeper models such as CNN5, 7 (mIOU = 75.66%, F1-score = 0.760) CNN8, 7 (mIOU = 77.20%, F1-score = 0.770) perfumed slightly worse than CNN5, 3 (mIOU = 76.53%, F1-score = 0.770). This is also true when using ResNet. The RES2, 3 outperformed the RES2, 4 and RES2, 7 on both mIOU and F1-score metrics.

Instead, feature-level fusion improved the results of detection regardless of model type and network depth (Figure 7). RES2, f performed the best by achieving 90.24% mIOU and 0.900 F1-score. CNN1, f was the second-best for the mIOU and F1-score metrics, respectively, with 83.27% and 0.830. The CNN8, f was slightly better on both metrics than the CNN5, f.

D. CNN AND RESNET ARCHITECTURE EVALUATION

Deeper models do not ensure better accuracy as demonstrated in the previous sub-section. Therefore, simply adding more layers to current models is not a useful solution for better landslide detection. Here we assessed the network ability for landslide detection when using different architectures like CNN and ResNet. Figure 8 summarizes the difference in landslide identification in the test area between ResNet and CNNs. ResNet exceeds any of the CNN models on the spectral dataset. It achieves 80.22% mIOU and 0.800 F1-score. The best CNN (8 layers) reached 77.86% mIOU and 0.780 F1-score. On the dataset that contained only the four topographical variables, CNN models showed better performance than the ResNet on the basis of mIOU. All the models had 0.670 F1-score. After stacking spectral and topographical layers together, ResNet showed a slightly better performance than the CNN models. The RES2, 7 achieved 77.28% mIOU and 0.770 F1-score. The results showed that deeper CNN models could better detect the landslides with this dataset. The CNN8, 7 had 77.20% mIOU and 0.770 F1-score compared to CNN1, 7 with 60.01% mIOU and 0.600 F1-score. In addition, ResNet significantly performed better than any of CNNs using the feature-level fusion for the spectral and topographical variables. On this dataset, a one-layer CNN performed better than deeper CNN models. RES2, f had 90.24% mIOU and 0.900 F1-score while CNN1, f could achieve 83.27% mIOU and 0.830 F1-score. Moreover, by examining the learning curves of the CNN and ResNet models (Figure 8c, 8d), it was noted that the latter converges faster to the best solution. Early termination has been used by monitoring the validation accuracy in 10 iterations to stop the training of the models. CNN1, 3 was trained for approximately 95 epochs, while the training of the RES2, 3 was completed in 46 epochs because of no validation accuracy improvements. The CNN model seems more stable than the ResNet from the graphs shown in Figure 1, but the latter has been more able to generalize into the test area in view of the mIOU and F1-score.

E. NETWORK DEPTH SENSITIVITY ANALYSIS

The depth of the network has an impact on landslide detection outcomes. We, therefore, studied the complexity of the models by the network depths to identify the landslides in the study area. A simple one-layer CNN convolution was applied at first. Then, two other models of depths 5 (two are convolutional) and 8 (three are convolutional) layers were compared with the simple one-layer CNN model. The assessment of these models demonstrates that if only spectral bands were used, deeper models perform better. The CNN8, 3 has 7% mIOU and 0.07 F1-score higher than the CNN1, 3. However, when only topographical variables were used, network depth was not impactful. The models with depth 3, 5, 8 all

TABLE 1. Accuracy evaluation of the LIM models researched based on the training and testing sites. Accuracies as overall accuracy, F1-score, and mIOU are indicated.

Model	Training Area		Testing Area	
	Training Accuracy	Validation Accuracy	F1-score	mIOU (%)
$CNN_{1,3}$	0.737	0.742	0.710	70.86
$CNN_{1,4}$	0.831	0.837	0.670	66.91
$CNN_{1,7}$	0.740	0.783	0.600	60.01
$CNN_{5,3}$	0.786	0.778	0.770	76.53
$CNN_{5,4}$	0.836	0.834	0.670	66.91
$CNN_{5,7}$	0.822	0.822	0.760	75.66
$CNN_{8,3}$	0.788	0.777	0.780	77.86
$CNN_{8,4}$	0.834	0.835	0.670	66.82
$CNN_{8,7}$	0.818	0.810	0.770	77.20
$RES_{2,3}$	0.764	0.818	0.800	80.22
$RES_{2,4}$	0.815	0.828	0.670	66.76
$RES_{2,7}$	0.825	0.782	0.770	77.28
$CNN_{1,f}$	0.831	0.840	0.830	83.27
$CNN_{5,f}$	0.824	0.810	0.790	78.63
$CNN_{8,f}$	0.834	0.805	0.800	79.94
$RES_{2,f}$	0.803	0.816	0.900	90.24

achieved 0.670 F1-score. The CNN8, 4 was slightly worse by the mIOU metric (66.82%) than the models with less depth size (66.91%). When both spectral bands and topographic variables were combined by stacking layers, deeper models showed better performance than using shallower networks. With CNN8, 7 (77.20% mIOU and 0.770 F1-score) significant improvements were noted to that of CNN1, 7 (60.01% mIOU and 0.600 F1-score). But with feature-level fusion, deeper models did not outperform the one-layer CNN model. Adding more convolutional layers or residual blocks could significantly improve the residual network accuracy.

F. OVERALL ASSESSMENT

Table 1 illustrates the quantitative assessment of the landslide detection results using overall accuracy for the training area (50% training, 50% validation) and F1-score and mIOU for the testing area. On the test area, the highest F1-score (0.900) and mIOU (90.24%) was obtained by the RES2, f followed by the CNN1, f with 0.830 F1-score and 83.27% mIOU. The worse F1-score (0.600) and mIOU (60.01%) was obtained by the CNN1, 7. CNN5, 4 achieved the best training accuracy (0.836) and CNN1, f achieved the best validation accuracy (0.840).

V. DISCUSSIONS AND CONCLUSIONS

Deep learning techniques, particularly convolutional networks, have shown to be successful in image recognition. They are also proved efficient for classifying remote sensing images, and other applications use spatial data. Recently, they outperformed other traditional machine learning methods for the detection of landslides [8]. However, designing appropriate network architecture, optimizing network parameters and choosing appropriate training strategies remain a challenging task. This paper presented landslide detection by residual networks, a kind of deep learning method that uses residual blocks, also known as skip connections, to improve computational and learning efficiency of deep networks. We also experimented with the applications of this network architecture and three other CNN baselines for the fusion of spectral bands obtained from aerial photographs and various topographical variables such as altitude, slope, aspect, and curvature.

The study of [8] showed extra topographical variables which did not promote the detection result compared to using spectral information. Only slope was found helpful to distinguish settlement areas from landslides. Using layer stacking, they combined spectral and topographical layers for their network input. This research contrasted such a fusion technique with feature-level fusion using a one-layer CNN, two other deeper CNNs, and a residual network. Layer stacking in our research also degraded the accuracy of such network models compared to using only spectral information regardless of network architecture and depth. Interestingly, all the same models (same architecture, same network depth, and the same parameters) showed better performance by feature-level fusion to using spectral information only. Residual architecture and one-layer CNN have benefitted most from such fusion for spectral and topographical variables. Our residual network performed better by 0.13 F1-score and 12.96% with feature-level fusion to layer stacking. The one-layer CNN with feature-level fusion also improved F1-score and mIOU by 0.23 and 23.26%, respectively, on the detection result by layer stacking. Due to this fusion approach, we also found slight improvements in the deeper CNNs.

Regarding network architecture design, residual design performed best on spectral dataset while CNN without residual blocks showed improved accuracy when using only topographical variables. As a consequence, network models should be designed according to the input dataset and its type of modality. Designing optimal network architectures becomes difficult when input data from different modalities are stacked together and deeper models perform better than their shallower counterparts. Instead, if feature-level fusion was used, residual designs are found significantly better than any of CNN designs. Residual networks converge faster to optimal networks than CNNs without residual blocks and generalize better to test areas. Moreover, CNN designs require extra attention when choosing network depth based on the input dataset. On the other hand, residual designs found better for adding more convolutional or dense layers to the network. Deep learning-based landslide detection can be fully automated and reliable with additional improvements to current network architectures, fusion strategies to combine data from various modalities, and designing networks that are stable and efficient with small training datasets. Further research, therefore, should focus on the presented network architectures by paying more attention to how such models learn abstract representations and merge them from different data modalities to detect landslides.

ACKNOWLEDGMENT

The authors would like to thank the Department of Mineral and Geosciences, the Department of Surveying Malaysia, and the Federal Department of Town and Country Planning.

REFERENCES

[1] A. Colombo, L. Lanteri, M. Ramasco, and C. Troisi, "Systematic GIS-based landslide inventory as the first step for effective landslide-hazard management," *Landslides*, vol. 2, no. 4, pp. 291–301, Dec. 2005.

[2] J. A. Palenzuela, M. Marsella, C. Nardinocchi, J. L. Pérez, T. Fernández, J. Chacón, and C. Irigaray, "Landslide detection and inventory by integrating LiDAR data in a GIS environment," *Landslides*, vol. 12, no. 6, pp. 1035–1050, Dec. 2015.

[3] Z. Li, W. Shi, P. Lu, L. Yan, Q. Wang, and Z. Miao, "Landslide mapping from aerial photographs using change detection-based Markov random field," *Remote Sens. Environ.*, vol. 187, pp. 76–90, Dec. 2016.

[4] B. Pradhan, M. I. Seeni, and H. Nampak, "Integration of LiDAR and quickbird data for automatic landslide detection using object-based analysis and random forests," in *Laser Scanning Applications in Landslide Assessment*, B. Pradhan, Ed. Cham, Switzerland: Springer, 2017, pp. 69–81.

[5] F. Chen, B. Yu, C. Xu, and B. Li, "Landslide detection using probability regression, a case study of Wenchuan, northwest of Chengdu," *Appl. Geography*, vol. 89, pp. 32–40, Dec. 2017.

[6] Z. Chen, Y. Zhang, C. Ouyang, F. Zhang, and J. Ma, "Automated landslides detection for mountain cities using multi-temporal remote sensing imagery," *Sensors*, vol. 18, no. 3, p. 821, Mar. 2018.

[7] A. C. Mondini, M. Santangelo, M. Rocchetti, E. Rossetto, A. Manconi, and O. Monserrat, "Sentinel-1 SAR amplitude imagery for rapid landslide detection," *Remote Sens.*, vol. 11, no. 7, p. 760, Mar. 2019.

[8] O. Ghorbanzadeh, T. Blaschke, K. Gholamnia, S. R. Meena, D. Tiede, and J. Aryal, "Evaluation of different machine learning methods and deep-learning convolutional neural networks for landslide detection," *Remote Sens.*, vol. 11, no. 2, p. 196, Jan. 2019.

[9] M. R. Mezaal and B. Pradhan, "Data mining-aided automatic landslide detection using airborne laser scanning data in densely forested tropical areas," *Korean J. Remote Sens.*, vol. 34, no. 1, pp. 45–74, 2018.

[10] B. Pradhan and S. Lee, "Landslide susceptibility assessment and factor effect analysis: Backpropagation artificial neural networks and their comparison with frequency ratio and bivariate logistic regression modelling," *Environ. Model. Softw.*, vol. 25, no. 6, pp. 747–759, Jun. 2010.

[11] A. Carrara, G. Crosta, and P. Frattini, "Geomorphological and historical data in assessing landslide hazard," *Earth Surf. Process. Landforms*, vol. 28, no. 10, pp. 1125–1142, Sep. 2003.

[12] F. Brardinoni, O. Slaymaker, and M. A. Hassan, "Landslide inventory in a rugged forested watershed: A comparison between air-photo and field survey data," *Geomorphology*, vol. 54, nos. 3–4, pp. 179–196, Sep. 2003.

[13] J. Nichol and M. S. Wong, "Detection and interpretation of landslides using satellite images," *Land Degradation Develop.*, vol. 16, no. 3, pp. 243–255, May 2005.

[14] M. Santangelo, M. Cardinali, M. Rossi, A. C. Mondini, and F. Guzzetti, "Remote landslide mapping using a laser rangefinder binocular and GPS," *Natural Hazards Earth Syst. Sci.*, vol. 10, no. 12, pp. 2539–2546, Dec. 2010.

[15] M. Galli, F. Ardizzone, M. Cardinali, F. Guzzetti, and P. Reichenbach, "Comparing landslide inventory maps," *Geomorphology*, vol. 94, nos. 3–4, pp. 268–289, Feb. 2008.

[16] Z. Li, W. Shi, S. W. Myint, P. Lu, and Q. Wang, "Semi-automated landslide inventory mapping from bitemporal aerial photographs using change detection and level set method," *Remote Sens. Environ.*, vol. 175, pp. 215–230, Mar. 2016.

[17] T. Lei, Y. Zhang, Z. Lv, S. Li, S. Liu, and A. K. Nandi, "Landslide inventory mapping from bitemporal images using deep convolutional neural networks," *IEEE Geosci. Remote Sens. Lett.*, vol. 16, no. 6, pp. 982–986, Jun. 2019.

[18] A. C. Mondini, F. Guzzetti, P. Reichenbach, M. Rossi, M. Cardinali, and F. Ardizzone, "Semi-automatic recognition and mapping of rainfall induced shallow landslides using optical satellite images," *Remote Sens. Environ.*, vol. 115, no. 7, pp. 1743–1757, Jul. 2011.

[19] T. Konishi and Y. Suga, "Landslide detection using COSMO-SkyMed images: A case study of a landslide event on Kii Peninsula, Japan," *Eur. J. Remote Sens.*, vol. 51, no. 1, pp. 205–221, Jan. 2018.

[20] G. Ventura, G. Vilardo, C. Terranova, and E. B. Sessa, "Tracking and evolution of complex active landslides by multi-temporal airborne LiDAR data: The Montaguto landslide (Southern Italy)," *Remote Sens. Environ.*, vol. 115, no. 12, pp. 3237–3248, Dec. 2011.

[21] D. T. Bui, H. Shahabi, A. Shirzadi, K. Chapi, M. Alizadeh, W. Chen, A. Mohammadi, B. B. Ahmad, M. Panahi, H. Hong, and Y. Tian, "Landslide detection and susceptibility mapping by AIRSAR data using support vector machine and index of entropy models in cameron Highlands, Malaysia," *Remote Sens.*, vol. 10, no. 10, p. 1527, Sep. 2018.

[22] B. Pradhan, M. N. Jebur, H. Z. M. Shafri, and M. S. Tehrany, "Data fusion technique using wavelet transform and Taguchi methods for automatic landslide detection from airborne laser scanning data and quickbird satellite imagery," *IEEE Trans. Geosci. Remote Sens.*, vol. 54, no. 3, pp. 1610–1622, Mar. 2016.

[23] S. Plank, A. Twele, and S. Martinis, "Landslide mapping in vegetated areas using change detection based on optical and polarimetric SAR data," *Remote Sens.*, vol. 8, no. 4, p. 307, Apr. 2016.

[24] I. Shaik, S. V. C. K. Rao, and B. Penta, "Detection of landslide using high resolution satellite data and analysis using entropy," in *Proc. Int. Conf. Remote Sens. Disaster Manage.*, P. Rao, K. Rao, and S. Kubo, Eds. Cham, Switzerland: Springer, 2019, pp. 243–250.

[25] M. Van Den Eeckhaut, J. Poesen, G. Verstraeten, V. Vanacker, J. Nyssen, J. Moeyersons, L. P. H. van Beek, and L. Vandekerckhove, "Use of LIDAR-derived images for mapping old landslides under forest," *Earth Surf. Process. Landforms*, vol. 32, no. 5, pp. 754–769, Apr. 2007.

[26] W. Chen, X. Li, Y. Wang, G. Chen, and S. Liu, "Forested landslide detection using LiDAR data and the random forest algorithm: A case study of the Three Gorges, China," *Remote Sens. Environ.*, vol. 152, pp. 291–301, Sep. 2014.

[27] P. V. Gorsevski, M. K. Brown, K. Panter, C. M. Onasch, A. Simic, and J. Snyder, "Landslide detection and susceptibility mapping using LiDAR and an artificial neural network approach: A case study in the Cuyahoga Valley National Park, Ohio," *Landslides*, vol. 13, no. 3, pp. 467–484, Jun. 2016.

[28] M. R. Mezaal, B. Pradhan, M. I. Sameen, H. Z. M. Shafri, and Z. M. Yusoff, "Optimized neural architecture for automatic landslide detection from high-resolution airborne laser scanning data," *Appl. Sci.*, vol. 7, no. 7, p. 730, Jul. 2017.

[29] J. Uemoto, T. Moriyama, A. Nadai, S. Kojima, and T. Umehara, "Landslide detection based on height and amplitude differences using pre- and post-event airborne X-band SAR data," *Natural Hazards*, vol. 95, no. 3, pp. 485–503, Oct. 2018.

[30] D. Di Martire, S. Tessitore, D. Brancato, M. G. Ciminelli, S. Costabile, M. Costantini, G. V. Graziano, F. Minati, M. Ramondini, and D. Calcaterra, "Landslide detection integrated system (LaDIS) based on *in-situ* and satellite SAR interferometry measurements," *CATENA*, vol. 137, pp. 406–421, Feb. 2016.

[31] A. Barra, O. Monserrat, M. Crosetto, M. Cuevas-Gonzalez, N. Devanthéry, G. Luzi, and B. Crippa, "Sentinel-1 data analysis for landslide detection and mapping: First experiences in Italy and Spain," in *Advancing Culture of Living with Landslides*, M. Mikoš, Ž. Arbanas, Y. Yin, and K. Sassa, Eds. Cham, Switzerland: Springer, 2017, pp. 201–208.

[32] J. Travelletti, J.-P. Malet, and C. Delacourt, "Image-based correlation of Laser Scanning point cloud time series for landslide monitoring," *Int. J. Appl. Earth Observ. Geoinf.*, vol. 32, pp. 1–18, Oct. 2014.

[33] J. Travelletti, C. Delacourt, P. Allemand, J.-P. Malet, J. Schmittbuhl, R. Toussaint, and M. Bastard, "Correlation of multi-temporal ground-based optical images for landslide monitoring: Application, potential and limitations," *ISPRS J. Photogram. Remote Sens.*, vol. 70, pp. 39–55, Jun. 2012.

[34] J.-Y. Rau, J.-P. Jhan, and R.-J. Rau, "Semiautomatic object-oriented landslide recognition scheme from multisensor optical imagery and DEM," *IEEE Trans. Geosci. Remote Sens.*, vol. 52, no. 2, pp. 1336–1349, Feb. 2014.

[35] A. Stumpf, J.-P. Malet, and C. Delacourt, "Correlation of satellite image time-series for the detection and monitoring of slow-moving landslides," *Remote Sens. Environ.*, vol. 189, pp. 40–55, Feb. 2017.

[36] A. Stumpf, J. P. Malet, P. Allemand, and P. Ulrich, "Surface reconstruction and landslide displacement measurements with Pléiades satellite images," *ISPRS J. Photogram. Remote Sens.*, vol. 95, pp. 1–12, Sep. 2014.

[37] R. N. Parker, A. L. Densmore, N. J. Rosser, M. de Michele, Y. Li, R. Huang, S. Whadcoat, and D. N. Petley, "Mass wasting triggered by the 2008 Wenchuan earthquake is greater than orogenic growth," *Nature Geosci.*, vol. 4, no. 7, pp. 449–452, May 2011.

[38] B. Yu, F. Chen, S. Muhammad, B. Li, L. Wang, and M. Wu, "A simple but effective landslide detection method based on image saliency," *Photogramm. Eng. Remote Sens.*, vol. 83, no. 5, pp. 351–363, May 2017.
[39] D. Lu, P. Mausel, E. Brondízio, and E. Moran, "Change detection techniques," *Int. J. Remote Sens.*, vol. 25, no. 12, pp. 2365–2401, 2004.
[40] F. Chen, B. Yu, and B. Li, "A practical trial of landslide detection from single-temporal Landsat8 images using contour-based proposals and random forest: A case study of national Nepal," *Landslides*, vol. 15, no. 3, pp. 453–464, Mar. 2018.
[41] U. C. Benz, P. Hofmann, G. Willhauck, I. Lingenfelder, and M. Heynen, "Multi-resolution, object-oriented fuzzy analysis of remote sensing data for GIS-ready information," *ISPRS J. Photogramm. Remote Sens.*, vol. 58, nos. 3–4, pp. 239–258, Jan. 2004.
[42] T. Blaschke, "Object based image analysis for remote sensing," *ISPRS J. Photogram. Remote Sens.*, vol. 65, no. 1, pp. 2–16, Jan. 2010.
[43] V. Lebourgeois, S. Dupuy, É. Vintrou, M. Ameline, S. Butler, and A. Bégué, "A combined random forest and OBIA classification scheme for mapping smallholder agriculture at different nomenclature levels using multisource data (simulated sentinel-2 time series, VHRS and DEM)," *Remote Sens.*, vol. 9, no. 3, p. 259, Mar. 2017.
[44] M. I. Sameen, B. Pradhan, H. Z. M. Shafri, M. R. Mezaal, and H. Bin Hamid, "Integration of ant colony optimization and object-based analysis for LiDAR data classification," *IEEE J. Sel. Topics Appl. Earth Observ. Remote Sens.*, vol. 10, no. 5, pp. 2055–2066, May 2017.
[45] B. Kalantar, S. B. Mansor, M. I. Sameen, B. Pradhan, and H. Z. Shafri, "Drone-based land-cover mapping using a fuzzy unordered rule induction algorithm integrated into object-based image analysis," *Int. J. Remote Sens.*, vol. 38, nos. 8–10, pp. 2535–2556, 2017.
[46] M. Kim, M. Madden, and T. Warner, "Estimation of optimal image object size for the segmentation of forest stands with multispectral IKONOS imagery," in *Object-Based Image Analysis*, T. Blaschke, S. Lang, and G. J. Hay, Eds. Berlin, Germany: Springer, 2008, pp. 291–307.
[47] T. R. Martha, N. Kerle, V. Jetten, C. J. van Westen, and K. V. Kumar, "Characterising spectral, spatial and morphometric properties of landslides for semi-automatic detection using object-oriented methods," *Geomorphology*, vol. 116, nos. 1–2, pp. 24–36, Mar. 2010.
[48] T. R. Martha, N. Kerle, C. J. V. Westen, V. Jetten, and K. V. Kumar, "Segment optimization and data-driven thresholding for knowledge-based landslide detection by object-based image analysis," *IEEE Trans. Geosci. Remote Sens.*, vol. 49, no. 12, pp. 4928–4943, Dec. 2011.
[49] A. Stumpf and N. Kerle, "Object-oriented mapping of landslides using random forests," *Remote Sens. Environ.*, vol. 115, no. 10, pp. 2564–2577, Oct. 2011.
[50] P. Lu, A. Stumpf, N. Kerle, and N. Casagli, "Object-oriented change detection for landslide rapid mapping," *IEEE Geosci. Remote Sens. Lett.*, vol. 8, no. 4, pp. 701–705, Jul. 2011.
[51] J. Dou, K.-T. Chang, S. Chen, A. P. Yunus, J.-K. Liu, H. Xia, and Z. Zhu, "Automatic case-based reasoning approach for landslide detection: Integration of object-oriented image analysis and a genetic algorithm," *Remote Sens.*, vol. 7, no. 4, pp. 4318–4342, Apr. 2015.
[52] C. Kurtz, A. Stumpf, J.-P. Malet, P. Gançarski, A. Puissant, and N. Passat, "Hierarchical extraction of landslides from multiresolution remotely sensed optical images," *ISPRS J. Photogram. Remote Sens.*, vol. 87, pp. 122–136, Jan. 2014.
[53] S. Plank, D. Hölbling, C. Eisank, B. Friedl, S. Martinis, and A. Twele, "Comparing object-based landslide detection methods based on polarimetric SAR and optical satellite imagery—A case study in Taiwan," in *Proc. 7th Int. Workshop Sci. Appl. SAR Polarimetry Polarimetric Interferometry*, 2015, pp. 1–5.
[54] M. R. Mezaal, B. Pradhan, and H. M. Rizeei, "Improving landslide detection from airborne laser scanning data using optimized Dempster–Shafer," *Remote Sens.*, vol. 10, no. 7, p. 1029, Jun. 2018.
[55] Y. S. Myint, P. Gober, A. Brazel, S. Grossman-Clarke, and Q. Weng, "Per-pixel vs. object-based classification of urban land cover extraction using high spatial resolution imagery," *Remote Sens. Environ.*, vol. 115, no. 5, pp. 1145–1161, May 2011.
[56] A. Ding, Q. Zhang, X. Zhou, and B. Dai, "Automatic recognition of landslide based on CNN and texture change detection," in *Proc. 31st Youth Acad. Annu. Conf. Chin. Assoc. Automat. (YAC)*, Nov. 2016, pp. 444–448.
[57] B. Pradhan, S. Lee, and M. F. Buchroithner, "A GIS-based back-propagation neural network model and its cross-application and validation for landslide susceptibility analyses," *Comput. Environ. Urban Syst.*, vol. 34, no. 3, pp. 216–235, May 2010.
[58] Y. LeCun, L. Bottou, Y. Bengio, and P. Haffner, "Gradient-based learning applied to document recognition," *Proc. IEEE*, vol. 86, no. 11, pp. 2278–2324, Nov. 1998.
[59] Y. LeCun, Y. Bengio, and G. Hinton, "Deep learning," *Nature*, vol. 521, no. 7553, pp. 436–444, May 2015.
[60] S. Ioffe and C. Szegedy, "Batch normalization: Accelerating deep network training by reducing internal covariate shift," 2015, *arXiv:1502.03167*. [Online]. Available: https://arxiv.org/abs/1502.03167
[61] K. He, X. Zhang, S. Ren, and J. Sun, "Deep residual learning for image recognition," in *Proc. IEEE Conf. Comput. Vis. Pattern Recognit. (CVPR)*, Jun. 2016, pp. 770–778.
[62] D. P. Kingma and J. Ba, "Adam: A method for stochastic optimization," 2014, *arXiv:1412.6980*. [Online]. Available: https://arxiv.org/abs/1412.6980

MAHER IBRAHIM SAMEEN was born in Dyala, Iraq, in 1990. He received the B.E. degree in surveying engineering from the Technical College of Kirkuk, Iraq, in 2011, the M.Sc. degree in remote sensing and GIS from Universiti Putra Malaysia (UPM), Selangor, Malaysia, in 2015, and the Ph.D. degree in remote sensing from UPM. He is currently a Postdoctoral Research Fellow with the School of Information Systems and Modelling, University of Technology Sydney (UTS). He is fueled by his passion for developing algorithms for remote sensing and geospatial applications. His background in surveying engineering, geomatics, and remote sensing informs his mindful but competitive approach. He participated in many international conferences and has published several ISI journal papers. His current research interests include GIS-based modeling, traffic accident analysis, and machine learning. He was a recipient of the Best Paper Award of the IEEE Workshop on Geoscience and Remote Sensing (IWGRS 2016), Malaysia.

BISWAJEET PRADHAN is the Director of the Centre for Advanced Modelling and Geospatial Information Systems (CAMGIS), Faculty of Engineering and IT, University of Technology Sydney, where he is also the Distinguished Professor. He is an internationally established Scientist in the field of geospatial information systems (GIS), remote sensing and image processing, complex modeling/geo-computing, machine learning and soft-computing applications, natural hazards, and environmental modeling. Out of his more than 462 articles, more than 400 have been published in science citation index (SCI/SCIE) technical journals. He has written eight books and 13 book chapters. He is listed as the World's Most Highly Cited Researcher by Clarivate Analytics Report, in 2018, 2017, and 2016 as one of the world's most influential mind. In 2018, he has been awarded as a World Class Professor by the Ministry of Research, Technology and Higher Education, Indonesia. He was a recipient of the Alexander von Humboldt Fellowship from Germany. He has received 55 awards, since 2006, in recognition of his excellence in teaching, service, and research. Since February 2015, he has been serving as an Ambassador Scientist for the Alexander Humboldt Foundation, Germany. He is an Associate Editor and an Editorial Member for more than eight ISI journals. He has widely traveled abroad visiting more than 52 countries to present his research findings.